THE JOURNAL OF PHYSICAL CHEMISTRY C
A JOURNAL OF THE AMERICAN CHEMICAL SOCIETY

pubs.acs.org/JPCC

Article

Conductor–Insulator Interfaces in Solid Electrolytes: A Design Strategy to Enhance Li-Ion Dynamics in Nanoconfined $LiBH_4/Al_2O_3$

Roman Zettl, Katharina Hogrefe, Bernhard Gadermaier, Ilie Hanzu, Peter Ngene, Petra E. de Jongh, and H. Martin R. Wilkening*

Cite This: *J. Phys. Chem. C* 2021, 125, 15052–15060

Read Online

ACCESS | Metrics & More | Article Recommendations | Supporting Information

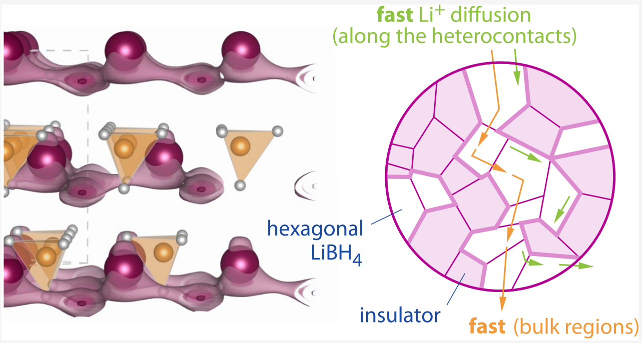

ABSTRACT: Synthesizing Li-ion-conducting solid electrolytes with application-relevant properties for new energy storage devices is a challenging task that relies on a few design principles to tune ionic conductivity. When starting with originally poor ionic compounds, in many cases, a combination of several strategies, such as doping or substitution, is needed to achieve sufficiently high ionic conductivities. For nanostructured materials, the introduction of conductor–insulator interfacial regions represents another important design strategy. Unfortunately, for most of the two-phase nanostructured ceramics studied so far, the lower limiting conductivity values needed for applications could not be reached. Here, we show that in nanoconfined $LiBH_4/Al_2O_3$ prepared by melt infiltration, a percolating network of fast conductor–insulator Li^+ diffusion pathways could be realized. These heterocontacts provide regions with extremely rapid ^7Li NMR spin fluctuations giving direct evidence for very fast Li^+ jump processes in both nanoconfined $LiBH_4/Al_2O_3$ and $LiBH_4$-LiI/Al_2O_3. Compared to the nanocrystalline, Al_2O_3-free reference system $LiBH_4$-LiI, nanoconfinement leads to a strongly enhanced recovery of the ^7Li NMR longitudinal magnetization. The fact that almost no difference is seen between $LiBH_4$-LiI/Al_2O_3 and $LiBH_4/Al_2O_3$ unequivocally reveals that the overall ^7Li NMR spin-lattice relaxation rates are solely controlled by the spin fluctuations near or in the conductor–insulator interfacial regions. Thus, the conductor–insulator nanoeffect, which in the ideal case relies on a percolation network of space charge regions, is independent of the choice of the bulk crystal structure of $LiBH_4$, either being orthorhombic ($LiBH_4/Al_2O_3$) or hexagonal ($LiBH_4$-LiI/Al_2O_3). ^7Li (and ^1H) NMR shows that rapid local interfacial Li-ion dynamics is corroborated by rather small activation energies on the order of only 0.1 eV. In addition, the LiI-stabilized layer-structured form of $LiBH_4$ guarantees fast two-dimensional (2D) bulk ion dynamics and contributes to facilitating fast long-range ion transport.

INTRODUCTION

Hydride-based solids attracted great attention as promising electrolytes for lithium-ion batteries[1] due to their compatibility with Li metal and their mechanical robustness.[2,3] While Li^+-ion transport in polycrystalline oxide-type electrolytes[4] may suffer from large grain-boundary resistances, such regions do not hinder long-range ion transport in the mechanically softer hydrides.[5]

The most prominent model hydride is $LiBH_4$ whose hexagonal modification, which is stable above T_{pt} = 110 °C, shows high conductivities in the mS cm^{-1} range.[6,7] The corresponding orthorhombic form, being the favorable crystal structure below T_{pt}, is, however, a rather poor ion conductor,[7] likely because of much higher defect formation energies.[8] While ultraslow Li^+ ion exchange in orthorhombic $LiBH_4$ is assumed to take place in three dimensions (Figure 1), for layer-structured $LiBH_4$, a two-dimensional (2D) conduction mechanism prevails (Figure 1), as has been shown by both frequency-dependent ^7Li NMR spin-lattice relaxation (SLR) measurements[9−11] and calculations.[12] This 2D diffusion behavior is illustrated in Figure 1 using bond valence site energy estimations.

Two approaches have been established and presented in the literature that successfully enhance the room-temperature ionic conductivity of $LiBH_4$ by several orders of magnitude, viz., (i) nanoconfinement of $LiBH_4$ in insulating oxides[13,14] and (ii) and partial cationic and especially anionic substitution[6,7] of the BH_4^- units with halogen ions like I^-, Br^-, or Cl^-. It is strongly anticipated that these two approaches lead to fundamentally

Received: April 28, 2021
Revised: June 22, 2021
Published: July 6, 2021

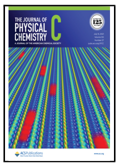

https://doi.org/10.1021/acs.jpcc.1c03789
J. Phys. Chem. C 2021, 125, 15052−15060

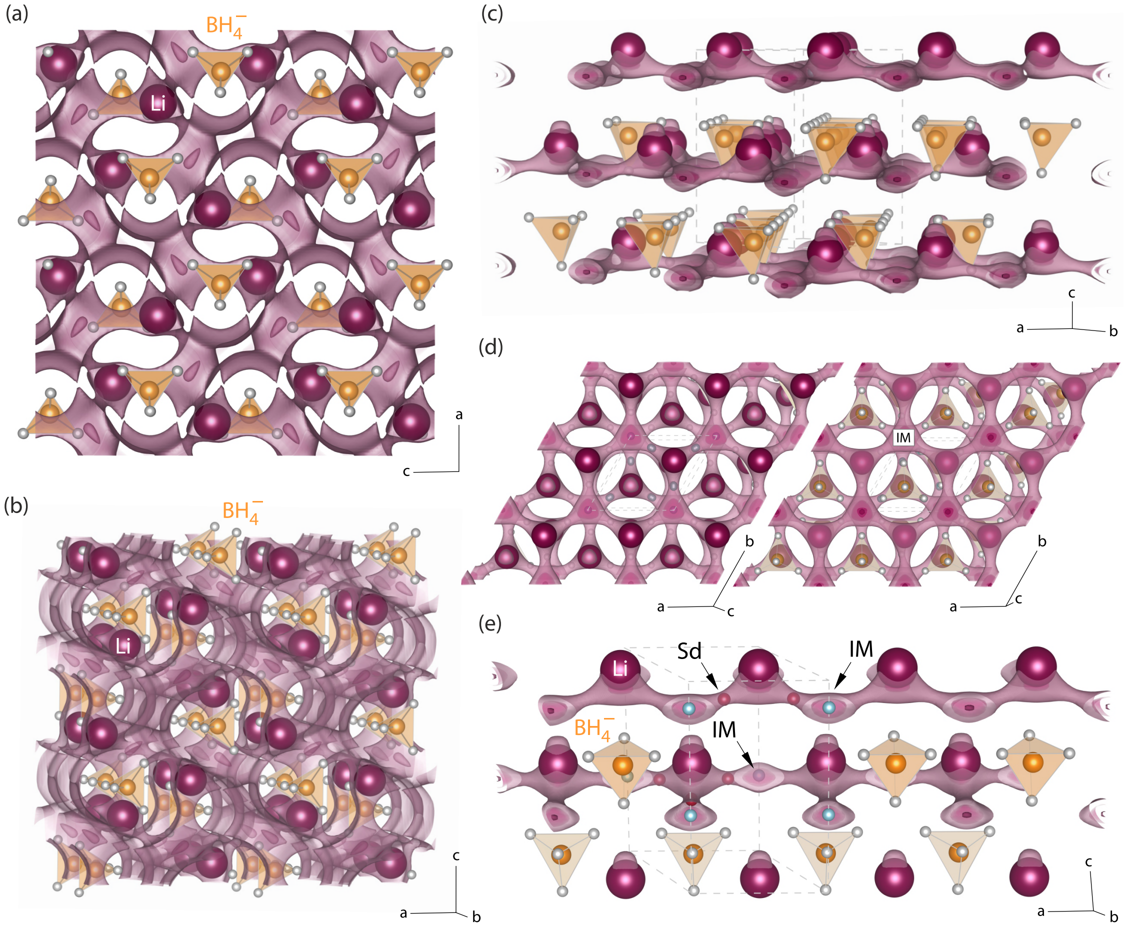

Figure 1. (a, b) Crystal structure of orthorhombic $LiBH_4$, slightly different viewing direction as indicated by the axes drawn. The topology of possible ion-migration paths, as estimated via the SoftBV software tool and the bond valence pathway analyzer (see text), turned out to be interrupted rather than interconnected, mirroring the poor ionic conductivity of this phase. (c−e) Crystal structure of layered, hexagonal $LiBH_4$ for which the Li^+ ions preferentially diffuse in two dimensions. (d) View along the *c*-axis in both directions to visualize the next-neighbor Li^+ jump processes on a hexagonal lattice. (e) When jumping between regularly occupied sites, the ions temporarily occupy an intermediate position (IM). The saddle points connecting IM with the regular sites are marked with Sd and represent the points of the highest energy along the migration path.

different diffusion mechanisms. While anion substitution in $LiBH_4$-LiX (X = I, Br, Cl) stabilizes the highly conductive hexagonal phase at much lower temperatures than T_{pt},[15] through nanoconfinement, a large fraction of Li^+-ion conductor−(ionic)insulator interfacial regions are introduced, which are suggested to be responsible for increased long-range ion transport. A definite proof of the latter concept or effect is, however, still missing for the $LiBH_4/Al_2O_3$ composites. For $LiBH_4/SiO_2$ nanocomposites, the important role of surface groups has been discussed recently.[16,17]

In general, heterocontacts between two different phases, viz., an ion conductor and an insulating phase, or even between two (mixed) conductors, may generate a percolation network of space charge regions with enhanced charge carrier mobility. The most prominent two-phase system is composed of alternating layers of F^--ion-conducting BaF_2 and CaF_2 with thicknesses of 9 nm, which were grown by molecular beam epitaxy.[18] The foundations of space charge zones in such nanostructured artificial ion conductors were laid by Maier,[19−22] explaining such nontrivial size effects that rely on overlapping space charge zones. $CuBr/Al_2O_3(TiO_2)$ composites, as studied by Knauth and co-workers,[23] belong to another group of such composites that show enhanced electrical conductivity.[24,25]

In the case of Li-ion conductors, Liang observed increased ionic conductivities in samples of LiI/Al_2O_3.[26] Later, for the nanocrystalline system Li_2O/X_2O_3 (X = B, Al), similar effects[27,28] were observed by ^7Li NMR SLR rate measurements.[29,30] Although enhanced Li^+ diffusivity was probed, the resulting conductivities[28] could not reach any practical benchmark needed to realize all-solid-state batteries equipped with ceramic electrolytes.

This situation is, however, different for nanoconfined $LiBH_4$-LiI/Al_2O_3 and $LiBH_4/Al_2O_3$, both showing ionic conductivities in the order of 10^{-4} S cm^{-1},[31] which is by more than a factor of 100 higher than in orthorhombic $LiBH_4$.[13] To understand the synthetic approaches and their impact on overall ionic transport, the role of the conductor−insulator interface in achieving such high conductivities needs to be studied in detail. Preferably, such studies should include spectroscopic methods[32] being sensitive to local Li^+ hopping processes in or near these interfacial areas. Here, we used ^7Li NMR spectroscopy to quantify the effect of the conductor−insulator interfacial regions in nanoconfined $LiBH_4$-LiI/Al_2O_3 and $LiBH_4/Al_2O_3$ prepared by melt infiltration. Although a recent ^{27}Al NMR study in our labs suggested that (unsaturated) penta-coordinated Al centers near the Al_2O_3 surface regions are involved in creating a defect-rich $LiBH_4/Al_2O_3$ interface,[33]

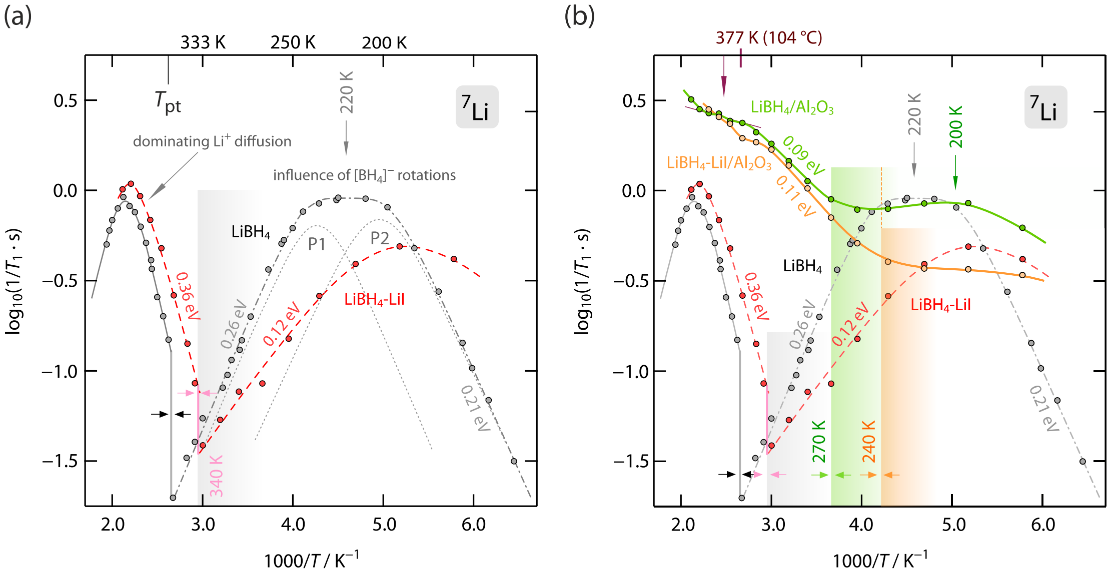

Figure 2. (a) Arrhenius representation of the ^{7}Li NMR spin-lattice relaxation rates $1/T_1$ (116 MHz) of microcrystalline $LiBH_4$ and the LiI-stabilized form $LiBH_4$-LiI; the former rates were taken from an earlier study by some of us.[9] Below the transition temperature of ca. 110 °C ($LiBH_4$, see gray area), the rates are governed by fast rotational BH_4^- dynamics in the orthorhombic form of $LiBH_4$. In hexagonal $LiBH_4$, $1/T_1$ is determined by Li$^+$ translational dynamics. For $LiBH_4$-LiI, the transformation temperature is reduced (see also (b)); furthermore, rotational dynamics gets enhanced as the ^{7}Li NMR rate peak is shifted toward lower temperatures, it appears at ca. 190 K. Solid and dashed lines are to guide the eye; see text for further details. (b) The same representation as in (a) but with the ^{7}Li NMR spin-lattice relaxation rates $1/T_1$ of the two nanoconfined samples included, viz., $LiBH_4$-LiI/Al_2O_3 and $LiBH_4/Al_2O_3$. Importantly, even for the sample free of any LiI, rather rapid Li$^+$ exchange processes are probed. This observation reveals the importance of the conductor−insulator interfacial regions determining overall ^{7}Li spin fluctuations in nanoconfined $LiBH_4/Al_2O_3$. Activation energies refer to the almost linear regions of the $1/T_1(1/T)$ dependence. Values as low as 0.1 eV point to an extremely flat potential landscape characterizing the conductor−insulator heterocontacts. See text for further explanation.

the ultimate proof via ^{7}Li NMR SLR measurements is still missing. In the present study, we directly compared the ^{7}Li (and ^{1}H) NMR response of longitudinal SLR of $LiBH_4$(-LiI)/Al_2O_3 with those of bulk $LiBH_4$ and LiI-stabilized $LiBH_4$. We observed a tremendous effect of the insulator Al_2O_3 on ^{7}Li NMR SLR, which is directly proportional to the diffusive motions of the Li$^+$ ions, clearly showing the superior role of conductor−insulator regions in solid electrolytes with nanometer-sized dimensions. Only in such samples, the volume fraction of these regions is large enough to have a dominant effect on overall ion transport properties.

Methods and Characterization. The composite electrolytes investigated here, i.e., $LiBH_4/Al_2O_3$ and $LiBH_4$-LiI/Al_2O_3, were prepared via melt infiltration; $LiBH_4$-LiI served as a reference compound. A detailed description of the corresponding procedure[34] as well as of the preparation and characterization of the composites[31] can be found elsewhere as the same samples were used for earlier studies. Ionic substitution was realized in a molar ratio of 80:20 ($LiBH_4$/LiI). The samples were kept at 295 °C for 30 min under 50 bar H_2 pressure in a stainless steel high-pressure autoclave (Parr). The average diameter of the pores in Al_2O_3 is in the order of 10 nm.[31] As mentioned above, at room temperature, bulk $LiBH_4$ crystallizes with orthorhombic structure and transforms into its hexagonal phase at temperatures higher than 110 °C; the corresponding X-ray diffraction patterns are shown in Figure S1. Here, results from differential scanning calorimetry (DSC), see Figure S2, reveal that the corresponding signal of $LiBH_4/Al_2O_3$ splits into two peaks at 103 °C and 114 °C; the signals are significantly decreased compared to the expected one of bulk $LiBH_4$, which was found at 117 °C. We do not observe any diagnostic DSC signals pointing to a phase change in $LiBH_4$-LiI/Al_2O_3 as for $LiBH_4$-LiI, the hexagonal modification is stabilized by the introduction of LiI already at lower temperatures. For the sake of completeness, $LiBH_4$-LiI shows a slight endothermic signal at −19 °C. The thermal behavior of $LiBH_4/Al_2O_3$ is useful when interpreting the diffusion-induced ^{7}Li NMR data, which were collected as follows.

Variable-temperature ^{7}Li (and ^{1}H) NMR $1/T_1$ SLR rates were measured with a Bruker Avance III 300 spectrometer that is connected to a 7-Tesla cryomagnet. The corresponding Larmor frequencies were 116 MHz for ^{7}Li and 300 MHz for ^{1}H. All samples were smoothly hand-pressed in Duran tubes under protective atmosphere and sealed. Relaxation rates were determined at temperatures ranging from −100 to 200 °C with an increment of usually 20 °C. In the region of the diffusion-induced rate peaks, additional ^{7}Li NMR $1/T_1$ rates were recorded every 10 or 5 °C. The laboratory-frame ^{7}Li (and ^{1}H) NMR $1/T_1$ rates were acquired with the well-known saturation recovery pulse sequence; depending on temperature, the 90° pulse lengths (200 W) varied from 2.5 to 2.9 μs (^{7}Li) and from 1.1 to 3.3 μs (^{1}H). Usually four to eight scans were accumulated to obtain a single free induction decay. For a detailed description of the pulse programs used and for a discussion of the procedure employed to parameterize the longitudinal NMR transients (partly displayed in Figure S3), we refer to our previous study.[33]

We also performed bond valence site energy estimations combined with a bond valence pathway analyzer using the softBV software tool developed by Adams and co-workers.[35,36] We took the structural information from published synchrotron X-ray powder diffraction data.[37] The softBV software executes a structure plausibility check, calculates surface energies, and gives information about the positions of interstitial sites and saddle points, as well as the topology and dimensionality of ion-migration paths and the respective migration barriers.[35,36] For the calculations, Li^+ was chosen as the mobile ion and the grid resolution was set to 0.1 Å. Pros and cons of the approach via softBV are discussed elsewhere.[36] For the visualization of the data, we used the VESTA software package.[38]

■ RESULTS AND DISCUSSION

NMR Spin-Lattice Relaxation: Li-Ion Translational Dynamics and Rotational Jumps of the Polyanions. As mentioned above, $LiBH_4$ crystallizes either with orthorhombic or with hexagonal symmetry. At temperatures lower than T_{pt} = 110 °C, the poorly conducting orthorhombic modification is present (see Figure 1). In ortho-$LiBH_4$, the ^7Li NMR spin-lattice relaxation rates indirectly sense the rapid rotational BH_4^- dynamics rather than Li^+ translational diffusion (see Figure 2a). Thus, at temperatures below T_{pt}, the ^7Li NMR rates pass through two rate peaks that mirror the two distinct rotational jump processes of the BH_4^- polyanions (see Figure 2a), which shows the ^7Li NMR SLR rates of coarse-grained, that is, microcrystalline $LiBH_4$. The broad rate maximum located at 220 K is composed of two individual rate peaks, which are represented by dotted lines and labeled P1 and P2 in Figure 2a. These rate peaks were analyzed in detail by both NMR[9,39,40] and quasi-elastic and inelastic neutron scattering earlier;[41] additionally, the mobility of boron atoms is discussed elsewhere.[42]

Above T_{pt}, the overall ^7Li NMR response in bulk $LiBH_4$ is governed by rapid Li^+ (translational) jump processes in the layer-structured form of $LiBH_4$. This dynamic process, which is 2D in nature as is illustrated in Figure 1, produces a single rate peak that points to an activation energy of 0.5 eV. In general, diffusion-induced ^7Li NMR rate peaks appear if the motional correlation rate $1/\tau_c$, which is expected within a factor of ca. 2 to be identical with the jump rate $1/\tau$, reaches the order of the (angular) Larmor frequency ω_0.[11] At the temperature where the peak appears, the condition $\omega_0\tau \approx 1$ is fulfilled.[43] A symmetric rate peak is only obtained for uncorrelated and isotropic (three-dimensional, 3D) diffusion. In many cases, structural disorder combined with Coulomb interactions results in asymmetric NMR peaks whose low-T flank shows a lower slope than that characterizing the flank on the high-T side.[43] Moreover, while the slope in the high-T regime is characteristic for long-range ion diffusion, the low-T flank of the peak is sensitive to short range, that is, local diffusion processes.[11]

Stabilizing the hexagonal phase of $LiBH_4$ by the incorporation of LiI leads to several changes of the overall ^7Li NMR response (see Figure 2a). First, it shifts the phase transition toward lower temperatures. Consequently, the ^7Li NMR $1/T_1(1/T)$ rates pass into the low-T flank of the rate peak, which characterizes translational Li^+, dynamics already at temperatures equal to or larger than 340 K. In agreement with faster Li^+ diffusion in $LiBH_4$-LiI, the slope of the low-temperature flank of the rate peak yields an activation energy E_a of 0.36 eV (Figure 2a) instead of 0.5 eV for $LiBH_4$.[9] This comparison shows that LiI does not only stabilize the hexagonal form at lower T but also reduces the mean activation barrier for Li^+ translational diffusion as it is seen by NMR (Figure 2a).

Apart from the change of the rates above T_{pt}, we recognize that also the rotational jump processes change when going from microcrystalline $LiBH_4$ to nanocrystalline $LiBH_4$-LiI. The original, overall maximum located at 220 K shifted toward a much lower temperature (Figure 2a), indicating an increase in the corresponding motional correlation rate sensed by the ^7Li spins. We assume that this increase is a direct consequence of the expanded lattice through the incorporation of I^- having a larger radius than BH_4^-. A deconvolution of this response into two rate peaks turned out to be no longer possible; for the LiI-containing sample $LiBH_4$-LiI, the former two rate peaks P1 and P2 (see above) merge into a much broader peak located at $T \approx$ 190 K. Most likely, this change originates from a broader distribution of rotational jump rates in $LiBH_4$-LiI. The shift toward lower temperatures agrees with a reduction of the activation energies E_a associated with the BH_4^- rotational jumps. Here, E_a decreases from 0.26 to 0.12 eV if we consider the high-T flank of the ^7Li NMR rate peaks just below T_{pt} (see Figure 2a). The introduction of LiI does also reduce the overall NMR coupling constant determining the maximum rates at T = 190 K.

Figure 2b shows the NMR responses of the two nanoconfined samples, $LiBH_4$-LiI/Al_2O_3 and $LiBH_4$/Al_2O_3. Starting from low temperatures, we recognize that the rates evolve in a similar manner to those of $LiBH_4$ and $LiBH_4$-LiI, respectively. However, especially for $LiBH_4$/Al_2O_3, without any LiI incorporated, we notice enhanced BH_4^- rotational dynamics compared to the microcrystalline reference sample $LiBH_4$ having no contact to any insulator phase. For $LiBH_4$-LiI/Al_2O_3 and $LiBH_4$-LiI, the ^7Li response turned out to be rather similar, while variable-temperature ^1H NMR SLR measurements (Figure S4) showed some subtle differences in this temperature regime (see the Supporting Information). As suggested by Figures S4 and 2b, rotational ion dynamics in or near the conductor−insulator interfacial regions are enhanced for $LiBH_4$(-LiI)/Al_2O_3 compared to those in the bulk regions of $LiBH_4$.

Most importantly, the largest effect of the insulating phase on ^7Li NMR spin-lattice relaxation is seen at higher temperatures when Li^+ translational ion dynamics start to govern the spin fluctuations (Figure 2b). In contrast to the sample without any Al_2O_3, we clearly recognize that the ^7Li NMR rates start to increase at temperatures as low as 240 and 270 K, respectively. These temperatures are clearly lower than T_{pt} = 340 K for $LiBH_4$-LiI (see Figure 2a). At temperatures slightly above 270 K, we recognize that the LiI-free sample does almost show the same NMR SLR response as seen for $LiBH_4$-LiI/Al_2O_3, which unequivocally reveals that the interface effect is the main reason for the longitudinal recovery of the magnetization mirroring Li^+ diffusivity.

Here, this effect turned out to be much larger than that seen for $LiBH_4$/Al_2O_3 composites that were earlier prepared by (high-energy) ball milling.[13] Melt infiltration leaves behind a defective $LiBH_4$ phase, and we assume tight conductor−insulator contacts. The nanoconfined samples provide a large fraction of these heterocontacts. Our comparative NMR results clearly show that the interfacial regions play a dominant role in explaining enhanced ion dynamics in the nanoconfined samples regardless of whether LiI is present or not. The latter finding is supported by recent calculations revealing that the poor ion transport in orthorhombic $LiBH_4$ originates from very high defect formation energies.[8] The $LiBH_4$/Al_2O_3 zones are, however, expected to be rich in defects, thus facilitating ion transport.[33] A similar effect has been described very recently by first-principles calculations for the interface in $LiBH_4$/MoS_2 composites.[44] Importantly, in $LiBH_4$/SiO_2 composites, the role of surface groups should not be underestimated.[16,17] Surface

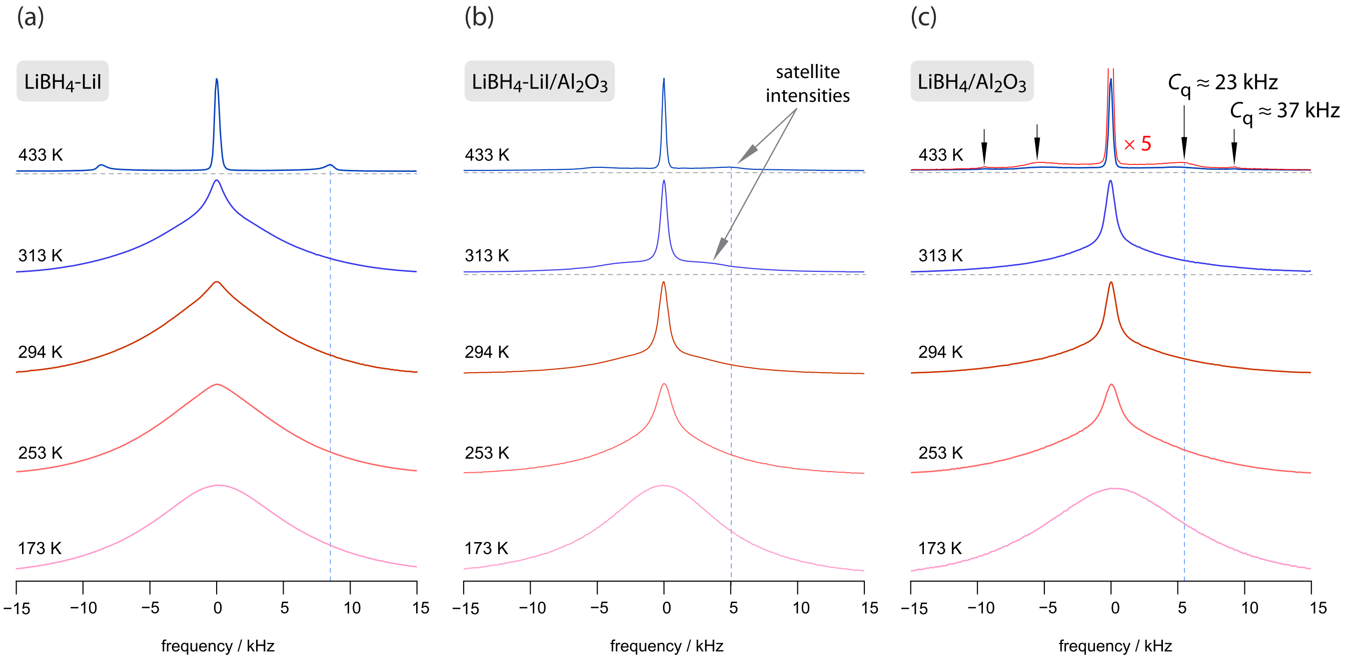

Figure 3. (a−c) Variable-temperature ^{7}Li NMR line shapes of the three samples studied, including the reference material $LiBH_4$-LiI. We observe distinct differences when the responses of the Al_2O_3-containing nanoconfined samples (see (b) and (c)) are compared with that of $LiBH_4$-LiI (a). For $LiBH_4$-LiI heterogeneous motional narrowing sets in at 294 K, stepwise narrowing is ascribed to two spin reservoirs with one of them representing the much less mobile Li^+ ions in the bulk regions crystallizing with orthorhombic structure at very low T. As LiI stabilizes the hexagonal form well above room temperature, the narrow line at elevated T reflects Li^+ ions in the hexagonal phase. For $LiBH_4$-LiI/Al_2O_3 and even for $LiBH_4$/Al_2O_3, the narrowing process is clearly shifted toward much lower temperatures of $T < 253$ K revealing that the conductor−Al_2O_3 interfacial regions govern overall Li^+ translational motions sensed by the ^{7}Li NMR spectra. Compared to the spectra shown in (a), a large fraction of Li ions benefits from this insulator or interface effect. The magnified spectrum in (c) shows the quadrupole powder pattern of $LiBH_4$/Al_2O_3. Dashed (vertical) lines refer to the position of the quadrupole singularities on the kHz scale; see text for further details.

effects are also important for $LiBH_4$/Al_2O_3: as has been shown quite recently by ^{27}Al NMR,[33] penta-coordinated Al centers Al^{IV} get saturated while generating $Al^{IV}BH_4^-$−Li^+, forming a defect-rich zone with vacant or interstitial Li^+ sites. The same mechanism has also been proposed by some of us for the recently studied LiF/Al_2O_3 nanocrystalline composites.[45]

Up to 330 K, the ^{7}Li NMR rates of the two nanoconfined Al_2O_3-containing samples (see Figure 2b) follow linear behavior. The associated activation energies turn out to be rather low and take values in the order of only 0.1 eV. This average value mirrors a flat potential landscape and is even lower than that of nanocrystalline $LiBH_4$ (0.18 eV) prepared by ball milling.[46] Values in the order of 0.07 eV were also observed indirectly by ^{1}H NMR SLR measurements above 380 K (see Figure S4, Supporting Information). Again, we ascribe the reduction in activation energy when going from nanostructured $LiBH_4$ to nanoconfined $LiBH_4$/Al_2O_3 to the interfacial "insulator effect" generating a percolation network of fast diffusion pathways for the Li^+ ions. Most likely, as detailed above, such a network benefits from defect-rich space charge regions that influence the Li^+ hopping processes.

The $1/T_1$ rates of nanoconfined $LiBH_4$/Al_2O_3 level off near 373 K and pass into a region that is characterized by a very low activation energy (see arrow in Figure 2b). In this region, the phase transition from orthorhombic to hexagonal $LiBH_4$ is marked by anisothermic peaks in our DSC measurements (see Figure S2, Supporting Information). As the addition of LiI stabilizes the hexagonal phase at temperatures well above room temperature, the anisothermic peaks are virtually absent. Again, this comparison shows that it is not the crystal structure but rather the interaction with the Al_2O_3 interfaces that governs ion dynamics in the interfacial regions of the nanoconfined composite samples below the phase transition temperature. Our results show how this effect can be used to turn a poor ion conductor, such as orthorhombic $LiBH_4$, into a superior material with fast Li^+ exchange processes assisting in facile macroscopic ionic transport (see below).

^{7}Li NMR Line Shapes of the Nanoconfined Composites. While NMR spin-lattice relaxation rates, especially when probed in the temperature regime of the low-T flank of the given $1/T_1(1/T)$ rate peak, are sensitive to the elementary hopping processes, NMR line shapes, which are governed by spin-spin-relaxation rates, can be used to probe Li^+ transport on longer length scales. To see whether and to which extent the conductor−insulator effect does also affect the corresponding ^{7}Li NMR lines, we recorded variable-temperature spectra of the reference sample $LiBH_4$-LiI (see Figure 3a) and the two nanoconfined samples (see Figure 3b,c).

Figure 3a shows the ^{7}Li NMR lines of nanocrystalline $LiBH_4$-LiI. Starting from a broad signal at 173 K, which reveals sluggish Li^+ translational ion dynamics in the bulk regions, the line undergoes heterogeneous motional narrowing upon heating. At temperatures above 294 K, a narrow line superimposes the broader Gaussian-shaped main signal. We attribute the narrowed line to Li^+ ions in the interfacial regions of this nanocrystalline sample. These regions offer fast Li^+ diffusion pathways as has recently been shown for nanocrystalline, orthorhombic $LiBH_4$.[46] The line recorded at 433 K reflects Li^+-ion dynamics in hexagonal $LiBH_4$-LiI. At this temperature, all Li^+ ions take part in rapid exchange processes. The quadrupolar satellite signals seen at ±8 kHz represent the 90° singularities of the powder pattern that is diagnostic for this sample. In general, quadrupole intensities mirror the interaction between the electric quadrupolar moment of the ^{7}Li nucleus (spin-quantum number I = 3/2) with a nonvanishing electric field gradient (EFG) at the nuclear site. This interaction alters the Zeeman levels such that for I = 3/2, four inequivalent levels are generated that depend on the crystallite orientation in the external magnetic field. Assuming an (averaged) axially symmetric EFG at the nuclear sites, the corresponding quadrupolar coupling constant C_q of the powder sample is given by C_q = 32 kHz.

Nanoconfinement, i.e., the introduction of conductor−insulator interfacial regions, ensures that (heterogeneous) motional narrowing does already set in at temperatures lower than 250 K. This temperature agrees with the temperature at which the ^{7}Li NMR rates start to increase. Satellite singularities come into the picture at 313 K. Already at 294 K, approximately 50% of the Li^+ ions in $LiBH_4$-LiI/Al_2O_3 (see Figure 3b) have access to fast diffusion pathways as is indicated by the ratio of the area fractions of the broad and the narrow NMR lines. For $LiBH_4/Al_2O_3$, the area fraction of the narrow line amounts to ca. 30% at 294 K (see Figure 3c).

As discussed earlier,[31,33] the overall coupling constant C_q (≈ 20 kHz) turned out to be clearly reduced compared to that of $LiBH_4$-LiI. Importantly, for $LiBH_4/Al_2O_3$, almost the same line shapes are detected as for the $LiBH_4$-LiI/Al_2O_3. Again, this result demonstrates the leading role of Al_2O_3 in governing the ^{7}Li NMR signals. Motional narrowing is slightly shifted toward higher T, which is in excellent agreement with the temperature behavior of the ^{7}Li NMR rates. The corresponding coupling constant C_q = 23 kHz of $LiBH_4$-Al_2O_3 resembles that of $LiBH_4$-LiI/Al_2O_3; see also the magnified spectrum recorded at 433 K (Figure 3c). It shows that nanoconfinement is also responsible for the electric quadrupole interactions and the majority of Li spins are subjected to in or near the conductor−insulator interfacial regions. As the pore size of Al_2O_3 is less than 10 nm, as has been reported earlier,[31] bulk regions, if confined to such small cages, are obviously also affected by the insulating surface regions.[31,33] The magnification of the spectrum recorded at 433 K (see Figure 3c) shows an additional pair of satellite regions, which we earlier ascribed to the Li ions farther away from the interface regions. The corresponding coupling constant of ca. 37 kHz agrees well with that which is obtained for pure $LiBH_4$ at this temperature. Hence, NMR is able to reveal the different electrical interactions the spins are sensing in nanoconfined $LiBH_4/Al_2O_3$, with most of them being subjected to the insulator surface interactions and some residing in the smaller bulk areas.[31] As mentioned above, this view is also corroborated by the NMR central lines shown in Figure 3.

Importantly, fast spin diffusion connecting the two spin reservoirs in the nanoconfined samples causes single exponential ^{7}Li NMR T_1 magnetization transients; thus, a separation of the two spin ensembles, as it was possible earlier for high-energy ball-milled $LiBH_4$, is almost impossible if we use the longitudinal transients for this purpose (see Figure S2). Moreover, at a given temperature, the associated $1/T_1$ ^{7}Li NMR rates of the fast and slowly decaying part of the underlying free indication decays do almost coincide. Hence, we conclude that for the nanometer-sized architecture in the conductor−insulator composites, rather efficient spin diffusion is present. Hence, from the point of view of SLR NMR, $LiBH_4$ in $LiBH_4/Al_2O_3$ appears as an almost homogeneous phase.

Noteworthy, while NMR is able to monitor the fast Li^+ exchange processes in the interfacial regions of the nanocomposites, it is, in the present case, less sensitive to long-range ion transport in $LiBH_4$-(LiI)/Al_2O_3. While the two samples $LiBH_4$-LiI/Al_2O_3 and $LiBH_4/Al_2O_3$ show almost the same ^{7}Li NMR response, through-going ionic transport in $LiBH_4$-LiI/Al_2O_3 is easier (ca. 1.3 × 10^{-4} S cm^{-1} (298 K))[31] than in $LiBH_4/Al_2O_3$ (0.3 × 10^{-4} S cm^{-1} (298 K)).[31] Most likely, this difference originates from the orthorhombic bulk regions in the latter compound that hinder Li^+ ion dynamics; see the schematic illustration in Figure 4 that summarizes the findings. A similar picture has been proposed for other dispersed ion conductors, such as nanocrystalline Li_2O/Al_2O_3 composites, whose heterogeneous transport properties were explained by the percolation concept.[47,48] Here, for both compounds, the $LiBH_4/Al_2O_3$ interface (heterocontacts) provides fast Li^+ diffusion pathways. While at low temperatures Li^+ diffusion in the orthorhombic bulk regions of $LiBH_4$ in $LiBH_4/Al_2O_3$ is slow, and only enhanced at the $LiBH_4/LiBH_4$ homocontacts, anion substitution in $LiBH_4$-LiI/Al_2O_3 additionally ensures fast Li^+ self-diffusivity in the hexagonal bulk regions that do not benefit from interactions with the surface regions. Therefore, the combination of nanoconfinement and anion substitution enables facile, overall Li^+ long-range ion transport as it is necessary for, e.g., battery applications.[31,33]

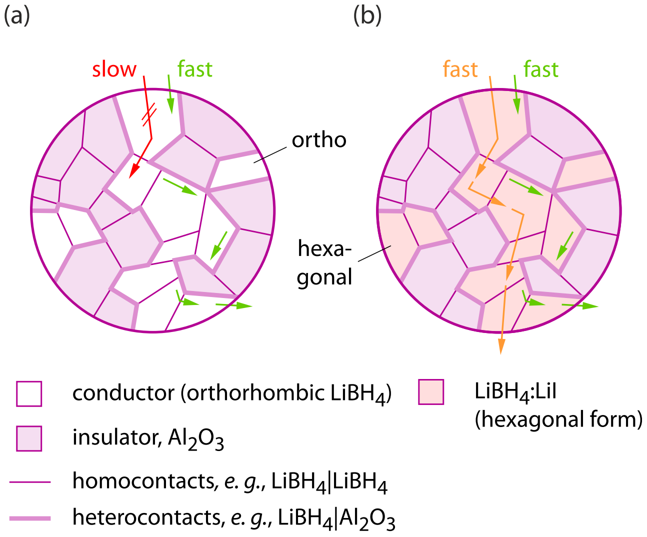

Figure 4. General schematic presentation of a system composed of two nanocrystalline phases, that is, an ionic conductor and a phase acting as an ionic insulator. (a) $LiBH_4/Al_2O_3$ and (b) $LiBH_4$-LiI/Al_2O_3 composites and the two different kinds of Li^+ diffusion pathways present. In both cases, ^{7}Li NMR is able to trace rapid fast Li^+ self-diffusivity along (or near) the interfacial pathways generated by the conductor−insulator heterocontacts. However, if no percolation pathways are formed, the poorly conducting orthorhombic phase hinders long-range (through-going) Li^+ ion transport (see (a)), whereas for $LiBH_4$-LiI/Al_2O_3, fast 2D Li^+ diffusion in the $LiBH_4$-LiI bulk regions[33] ensures facile long-range cation motions. As ionic conductivity depends on both the mobility μ and the charge carrier density N, the combination of anion substitution and nanoconfinement is a perfect tool to tune overall Li^+ transport.[31,33]

■ CONCLUSIONS

Using $LiBH_4$ and nanoconfined $LiBH_4$-LiI as model systems, we investigated the influence of conductor−insulator interfacial regions on the overall Li^+ translational ion dynamics, which we sensed by ^7Li NMR spin fluctuations. Al_2O_3 served as an insulating phase, that is, the phase usually blocking Li^+-ion transport. As irregular diffusive motions trigger (longitudinal) ^7Li NMR spin-lattice relaxation, with the help of variable-temperature measurements, activation energies and motional correlation rates can be probed.

While in nanoconfined $LiBH_4$-LiI rapid Li^+ translational motions (0.36 eV) influence the ^7Li NMR rates $1/T_1$ at temperatures above 340 K, in the Al_2O_3-bearing nanoconfined samples, a drastic change in overall NMR response is seen. For $LiBH_4$-LiI/Al_2O_3, the low-T flank of the corresponding diffusion-induced rate peak $1/T_1(1/T)$ is already seen at a temperature as low as 240 K, thus shifted by 100 K toward lower temperatures. Surprisingly, above 270 K, the same flank is also seen for the LiI-free sample unequivocally showing that the conductor−insulator (Al_2O_3) effect has the authoritative role to explain the enhanced Li^+-ion dynamics in these samples. Clearly, reduced activation energies in the order of only 0.1 eV agree with the low onset temperatures and underpin the idea of a percolation network of fast diffusion pathways generated by the conductor−insulator interfacial regions.

^7Li NMR line shape measurements corroborate the results from ^7Li NMR relaxometry and reveal, for both samples $LiBH_4$-LiI/Al_2O_3 and $LiBH_4/Al_2O_3$, an ensemble of mobile Li^+ ions being subjected to rapid diffusive motions already at temperatures well below ambient. ^7Li NMR quadrupole interactions seen in the spectra of nanoconfined $LiBH_4/Al_2O_3$ do reflect both bulk and interfacial regions, with the spins in the latter areas being highly mobile and benefiting from the interaction with the insulator surface. Our work highlights the importance of conductor−insulator interfacial regions in advanced solid electrolyte research. The clever introduction of such artificial interfaces, influencing ion dynamics by both structural disorder and space charge regions, represents an adjustable tool to manipulate overall (Li^+)ion dynamics in solids with nanometer-sized dimensions.

■ ASSOCIATED CONTENT

Supporting Information

The Supporting Information is available free of charge at https://pubs.acs.org/doi/10.1021/acs.jpcc.1c03789.

> ^7Li and ^1H NMR magnetization transients, ^1H NMR rates, DSC curves, and XRD patterns (PDF)

■ AUTHOR INFORMATION

Corresponding Author

H. Martin R. Wilkening − *Institute for Chemistry and Technology of Materials, Christian-Doppler-Laboratory for Lithium Batteries, Graz University of Technology (NAWI Graz), 8010 Graz, Austria;* orcid.org/0000-0001-9706-4892; Email: wilkening@tugraz.at

Authors

Roman Zettl − *Institute for Chemistry and Technology of Materials, Christian-Doppler-Laboratory for Lithium Batteries, Graz University of Technology (NAWI Graz), 8010 Graz, Austria; Materials Chemistry and Catalysis, Debye Institute for Nanomaterials Science, Utrecht University, 3584 Utrecht, Netherlands*

Katharina Hogrefe − *Institute for Chemistry and Technology of Materials, Christian-Doppler-Laboratory for Lithium Batteries, Graz University of Technology (NAWI Graz), 8010 Graz, Austria*

Bernhard Gadermaier − *Institute for Chemistry and Technology of Materials, Christian-Doppler-Laboratory for Lithium Batteries, Graz University of Technology (NAWI Graz), 8010 Graz, Austria;* orcid.org/0000-0003-2917-1818

Ilie Hanzu − *Institute for Chemistry and Technology of Materials, Christian-Doppler-Laboratory for Lithium Batteries, Graz University of Technology (NAWI Graz), 8010 Graz, Austria;* orcid.org/0000-0002-9260-9117

Peter Ngene − *Materials Chemistry and Catalysis, Debye Institute for Nanomaterials Science, Utrecht University, 3584 Utrecht, Netherlands;* orcid.org/0000-0003-3691-0623

Petra E. de Jongh − *Materials Chemistry and Catalysis, Debye Institute for Nanomaterials Science, Utrecht University, 3584 Utrecht, Netherlands;* orcid.org/0000-0002-2216-2620

Complete contact information is available at: https://pubs.acs.org/10.1021/acs.jpcc.1c03789

Notes

The authors declare no competing financial interest.

■ ACKNOWLEDGMENTS

H.M.R.W. thanks the German Science Foundation (Deutsche Forschungsgemeinschaft (DFG)) for financial support (research unit FOR1277). In addition, P.E.d.J. and P.N. acknowledge financial support by the Dutch Research Council (Nederlandse Organisatie voor Wetenschappelijk Onderzoek (NOW)), ECHO grant 712.015.005, as well as by the NWO materials for sustainability (Mat4Sus-739.017.009) grant. Moreover, further financial support by the Austrian Federal Ministry of Science, Research and Economy (BMWFW) and the National Foundation for Research, Technology and Development (CD-Laboratory of Lithium Batteries: Ageing Effects, Technology and New Materials) is gratefully acknowledged. This work also received funding from the European H2020 Framework program, no. 769929, and from the FFG comet project safe battery.

■ REFERENCES

(1) Bachman, J. C.; Muy, S.; Grimaud, A.; Chang, H. H.; Pour, N.; Lux, S. F.; Paschos, O.; Maglia, F.; Lupart, S.; Lamp, P.; et al. Inorganic Solid-State Electrolytes for Lithium Batteries: Mechanisms and Properties Governing Ion Conduction. *Chem. Rev.* **2016**, *116*, 140−162.

(2) de Jongh, P. E.; Blanchard, D.; Matsuo, M.; Udovic, T. J.; Orimo, S. Complex Hydrides as Room-Temperature Solid Electrolytes for Rechargeable Batteries. *Appl. Phys. A* **2016**, *122*, No. 251.

(3) Gulino, V.; Brighi, M.; Murgia, F.; Ngene, P.; de Jongh, P.; Černý, R.; Baricco, M. Room-Temperature Solid-State Lithium-Ion Battery Using a $LiBH_4$-MgO Composite Electrolyte. *ACS Appl. Energy Mater.* **2021**, *4*, 1228−1236.

(4) Thangadurai, V.; Narayanan, S.; Pinzaru, D. Garnet-Type Solid-State Fast Li Ion Conductors for Li Batteries: Critical Review. *Chem. Soc. Rev.* **2014**, *43*, 4714−4727.

(5) Manthiram, A.; Yu, X. W.; Wang, S. F. Lithium Battery Chemistries Enabled by Solid-State Electrolytes. *Nat. Rev. Mater.* **2017**, *2*, No. 16103.

(6) Matsuo, M.; Takamura, H.; Maekawa, H.; Li, H. W.; Orimo, S. Stabilization of Lithium Superionic Conduction Phase and Enhance-

ment of Conductivity of $LiBH_4$ by LiCl Addition. *Appl. Phys. Lett.* **2009**, *94*, No. 084103.

(7) Maekawa, H.; Matsuo, M.; Takamura, H.; Ando, M.; Noda, Y.; Karahashi, T.; Orimo, S. I. Halide-Stabilized $LiBH_4$, a Room-Temperature Lithium Fast-Ion Conductor. *J. Am. Chem. Soc.* **2009**, *131*, 894−895.

(8) Lee, Y.-S.; Cho, Y. W. Fast Lithium Ion Migration in Room Temperature $LiBH_4$. *J. Phys. Chem. C* **2017**, *121*, 17773−17779.

(9) Epp, V.; Wilkening, M. Fast Li Diffusion in Crystalline $LiBH_4$ due to Reduced Dimensionality: Frequency-Dependent NMR Spectroscopy. *Phys. Rev. B* **2010**, *82*, No. 020301.

(10) Volgmann, K.; Epp, V.; Langer, J.; Stanje, B.; Heine, J.; Nakhal, S.; Lerch, M.; Wilkening, M.; Heitjans, P. Solid-State NMR to Study Translational Li Ion Dynamics in Solids with Low-Dimensional Diffusion Pathways. *Z. Phys. Chem.* **2017**, *231*, 1215−1241.

(11) Uitz, M.; Epp, V.; Bottke, P.; Wilkening, M. Ion Dynamics in Solid Electrolytes for Lithium Batteries. *J. Electroceram.* **2017**, *38*, 142−156.

(12) Ikeshoji, T.; Tsuchida, E.; Morishita, T.; Ikeda, K.; Matsuo, M.; Kawazoe, Y.; Orimo, S.-I. Fast Ionic Conductivity of Li^+ in $LiBH_4$. *Phys. Rev. B* **2011**, *83*, No. 144301.

(13) Epp, V.; Wilkening, M. Motion of Li^+ in Nanoengineered $LiBH_4$ and $LiBH_4/Al_2O_3$ Comparison with the Microcrystalline Form. *Chem. Phys. Chem.* **2013**, *14*, 3706−3713.

(14) Blanchard, D.; Nale, A.; Sveinbjornsson, D.; Eggenhuisen, T. M.; Verkuijlen, M. H. W.; Suwarno; Vegge, T.; Kentgens, A. P. M.; de Jongh, P. E. Nanoconfined $LiBH_4$ as a Fast Lithium Ion Conductor. *Adv. Funct. Mater.* **2015**, *25*, 184−192.

(15) Oguchi, H.; Matsuo, M.; Hummelshoj, J. S.; Vegge, T.; Norskov, J. K.; Sato, T.; Miura, Y.; Takamura, H.; Maekawa, H.; Orimo, S. Experimental and Computational Studies on Structural Transitions in the $LiBH_4$-LiI Pseudobinary System. *Appl. Phys. Lett.* **2009**, *94*, No. 141912.

(16) Choi, Y. S.; Lee, Y. S.; Oh, K. H.; Cho, Y. W. Interface-Enhanced Li Ion Conduction in a $LiBH_4$-SiO_2 Solid Electrolyte. *Phys. Chem. Chem. Phys.* **2016**, *18*, 22540−22547.

(17) Ngene, P.; Lambregts, S. F. H.; Blanchard, D.; Vegge, T.; Sharma, M.; Hagemann, H.; de Jongh, P. E. The Influence of Silica Surface Groups on the Li-Ion Conductivity of $LiBH_4/SiO_2$ Nanocomposites. *Phys. Chem. Chem. Phys.* **2019**, *21*, 22456−22466.

(18) Sata, N.; Eberman, K.; Eberl, K.; Maier, J. Mesoscopic Fast Ion Conduction in Nanometre-Scale Planar Heterostructures. *Nature* **2000**, *408*, 946−949.

(19) Maier, J. Nanoionics: Ionic Charge Carriers in Small Systems. *Phys. Chem. Chem. Phys.* **2009**, *11*, 3011−3022.

(20) Maier, J. Nanoionics: Ion Transport and Electrochemical Storage in Confined Systems. *Nat. Mater.* **2005**, *4*, 805−815.

(21) Maier, J. Nano-Ionics: More Than Just a Fashionable Slogan. *J. Electroceram.* **2004**, *13*, 593−598.

(22) Maier, J. Nano-Ionics: Trivial and Non-Trivial Size Effects on Ion Conduction in Solids. *Z. Phys. Chem.* **2003**, *217*, 415−436.

(23) Knauth, P.; Schoonman, J. *Nanocomposites—Ionic Conducting Materials and Structural Spectroscopies*; Springer: New York, 2008.

(24) Knauth, P.; Debierre, J. M.; Albinet, G. Electrical Conductivity of Model Composites of an Ionic Conductor (CuBr) and an Insulator (TiO_2, Al_2O_3): Experiments and Percolation-Type Model. *Solid State Ionics* **1999**, *121*, 101−106.

(25) Knauth, P.; Albinet, G.; Debierre, J. M. Enhanced Electrical Conductivity of CuBr-TiO_2 Composites: Dependence on Temperature, Volume Fractions and Grain Sizes. *Ber. Bunsenges. Phys. Chem.* **1998**, *102*, 945−952.

(26) Liang, C. C. Conduction Charactersitics of Lithium Iodide Aluminium Oxide Solid Electrolytes. *J. Electrochem. Soc.* **1973**, *120*, 1289−1292.

(27) Indris, S.; Heitjans, P.; Ulrich, M.; Bunde, A. AC and DC Conductivity in Nano- and Microcrystalline Li_2O:B_2O_3 Composites: Experimental Results and Theoretical Models. *Z. Phys. Chem.* **2005**, *219*, 89−103.

(28) Indris, S.; Heitjans, P.; Roman, H. E.; Bunde, A. Nanocrystalline versus Microcrystalline Li_2O:B_2O_3 Composites: Anomalous Ionic Conductivities and Percolation Theory. *Phys. Rev. Lett.* **2000**, *84*, 2889−2892.

(29) Wilkening, M.; Indris, S.; Heitjans, P. Heterogeneous Lithium Diffusion in Nanocrystalline Li_2O/Al_2O_3 Composites. *Phys. Chem. Chem. Phys.* **2003**, *5*, 2225−2231.

(30) Indris, S.; Heitjans, P. Heterogeneous ^{7}Li NMR Relaxation in Nanocrystalline Li_2O:B_2O_3 Composites. *J. Non-Cryst. Solids* **2002**, *307−310*, 555−564.

(31) Zettl, R.; de Kort, L.; Gombotz, M.; Wilkening, H. M. R.; de Jongh, P. E.; Ngene, P. Combined Effects of Anion Substitution and Nanoconfinement on the Ionic Conductivity of Li-Based Complex Hydrides. *J. Phys. Chem. C* **2020**, *124*, 2806−2816.

(32) Verkuijlen, M. H. W.; Ngene, P.; de Kort, D. W.; Barré, C.; Nale, A.; van Eck, E. R. H.; van Bentum, P. J. M.; de Jongh, P. E.; Kentgens, A. P. M. Nanoconfined $LiBH_4$ and Enhanced Mobility of Li^+ and BH_4^- Studied by Solid-State NMR. *J. Phys. Chem. C* **2012**, *116*, 22169−22178.

(33) Zettl, R.; Gombotz, M.; Clarkson, D.; Greenbaum, S. G.; Ngene, P.; de Jongh, P. E.; Wilkening, H. M. R. Li-Ion Diffusion in Nanoconfined $LiBH_4$-LiI/Al_2O_3: From 2D Bulk Transport to 3D Long-Range Interfacial Dynamics. *ACS Appl. Mater. Interfaces* **2020**, *12*, 38570−38583.

(34) Suwarno, S.; Ngene, P.; Nale, A.; Eggenhuisen, T. M.; Oschatz, M.; Embs, J. P.; Remho, A.; de Jongh, P. E. Confinement Effects for Lithium Borohydride: Comparing Silica and Carbon Scaffolds. *J. Phys. Chem. C* **2017**, *121*, 4197−4205.

(35) Wong, L. L.; Phuah, K. C.; Dai, R.; Chen, H.; Chew, W. S.; Adams, S. Bond Valence Pathway Analyzer—An Automatic Rapid Screening Tool for Fast Ion Conductors within softBV. *Chem. Mater.* **2021**, *33*, 625−641.

(36) Chen, H.; Wong, L. L.; Adams, S. SoftBV—A Software Tool for Screening the Materials Genome of Inorganic Fast Ion Conductors. *Acta Crystallogr., Sect. B: Struct. Sci., Cryst. Eng. Mater.* **2019**, *75*, 18−33.

(37) Soulié, J. P.; Renaudin, G.; Černý, R.; Yvon, K. Lithium Boro-Hydride $LiBH_4$: I. Crystal Structure. *J. Alloys Compd.* **2002**, *346*, 200−205.

(38) Momma, K.; Izumi, F. VESTA 3 for Three-Dimensional Visualization of Crystal, Volumetric and Morphology Data. *J. Appl. Crystallogr.* **2011**, *44*, 1272−1276.

(39) Soloninin, A. V.; Skripov, A. V.; Buzlukov, A. L.; Stepanov, A. P. Nuclear Magnetic Resonance Study of Li and H Diffusion in the High-Temperature Solid Phase of $LiBH_4$. *J. Solid State Chem.* **2009**, *182*, 2357−2361.

(40) Skripov, A. V.; Soloninin, A. V.; Filinchuk, Y.; Chernyshov, D. Nuclear Magnetic Resonance Study of the Rotational Motion and the Phase Transition in $LiBH_4$. *J. Phys. Chem. C* **2008**, *112*, 18701−18705.

(41) Martelli, P.; Remhof, A.; Borgschulte, A.; Ackermann, R.; Strässle, T.; Embs, J. P.; Ernst, M.; Matsuo, M.; Orimo, S.-I.; Züttel, A. Rotational Motion in $LiBH_4$/LiI Solid Solutions. *J. Phys. Chem. A* **2011**, *115*, 5329−5334.

(42) Corey, R. L.; Shane, D. T.; Bowman, R. C.; Conradi, M. S. Atomic Motions in $LiBH_4$ by NMR. *J. Phys. Chem. C* **2008**, *112*, 18706−18710.

(43) Wilkening, M.; Heitjans, P. From Micro to Macro: Access to Long-Range Li^+ Diffusion Parameters in Solids via Microscopic ^{6,7}Li Spin-Alignment Echo NMR Spectroscopy. *Chem. Phys. Chem.* **2012**, *13*, 53−65.

(44) Liu, Z.; Xiang, M.; Zhang, Y.; Shao, H.; Zhu, Y.; Guo, X.; Li, L.; Wang, H.; Liu, W. Lithium Migration Pathways at the Composite Interface of $LiBH_4$ and Two-Dimensional MoS_2 Enabling Superior Ionic Conductivity at Room Temperature. *Phys. Chem. Chem. Phys.* **2020**, *22*, 4096−4105.

(45) Breuer, S.; Pregartner, V.; Lunghammer, S.; Wilkening, H. M. R. Dispersed Solid Conductors: Fast Interfacial Li-Ion Dynamics in

Nanostructured LiF and LiF:γ-Al_2O_3 Composites. *J. Phys. Chem. C* **2019**, *123*, 5222−5230.

(46) Breuer, S.; Uitz, M.; Wilkening, H. M. R. Rapid Li Ion Dynamics in the Interfacial Regions of Nanocrystalline Solids. *J. Phys. Chem. Lett.* **2018**, *9*, 2093−2097.

(47) Heitjans, P.; Wilkening, M. Ion Dynamics at Interfaces: Nuclear Magnetic Resonance Studies. *MRS Bull.* **2009**, *34*, 915−922.

(48) Roman, H. E.; Bunde, A.; Dieterich, W. Conductivity of Dispersed Ionic Conductors—a Percolation Model with 2 Critical Points. *Phys. Rev. B* **1986**, *34*, 3439−3445.